Research Square

Preprints are preliminary reports that have not undergone peer review.
They should not be considered conclusive, used to inform clinical practice,
or referenced by the media as validated information.

Intrinsic Sampling-Aware Discrete-Time Geometric Backstepping for Aggressive Quadrotor Tracking on SO(3)

Yuan Cao
Polytechnic University of Turin
Alessandro Rizzo
alessandro.rizzo@polito.it
Polytechnic University of Turin

Research Article

Keywords: Quadrotor, nonlinear control, discretetime control, geometric control, backstepping, SO(3)

Posted Date: May 31st, 2026

DOI: https://doi.org/10.21203/rs.3.rs-9838244/v1

License: This work is licensed under a Creative Commons Attribution 4.0 International License.
Read Full License

Additional Declarations: No competing interests reported.

Intrinsic Sampling-Aware Discrete-Time Geometric Backstepping for Aggressive Quadrotor Tracking on SO(3)

Cao Yuan[1] and Alessandro Rizzo[1]

***Abstract*—This paper addresses a well-recognized inconsistency arising in sampled implementations of nonlinear geometric control: continuous-time (CT) Lyapunov stability does not, in general, guarantee a decreasing discrete-time (DT) Lyapunov difference under non-negligible sampling effects, potentially leading to discrepancies between predicted and implemented closed-loop behavior. To resolve this issue for quadrotor trajectory tracking, an intrinsic DT geometric backstepping framework is developed on $\mathsf{SO}(3)$ that explicitly accounts for sampling effects while preserving the Lie-group structure of the attitude dynamics. The proposed framework resolves the noncausal dependence inherent in DT backstepping through a structure-preserving geometric predictor that enables causal one-step matching directly on $\mathsf{SO}(3)$. Geometric consistency is preserved through a Lie-group formulation, while a rigorous DT Lyapunov difference analysis explicitly characterizes sampling-dependent stability properties arising from finite-step residual effects. The analysis establishes global exponential stability of the translational subsystem and Semi-Globally Uniformly Ultimately Bounded (SGUUB) of the rotational tracking errors with sampling-dependent margins. Simulations demonstrate accurate tracking under aggressive maneuvers, machine-precision preservation of $\mathsf{SO}(3)$ orthogonality, and closed-loop behavior consistent with theoretical sampling bounds, supporting the effectiveness of intrinsic DT design for achieving sampling-consistent closed-loop behavior under practical sampling conditions.**

***Index Terms*—Quadrotor, nonlinear control, discrete-time control, geometric control, backstepping, SO(3).**

I. Introduction

Unmanned Aerial Vehicles (UAVs) have been widely deployed in complex missions such as reconnaissance and search-and-rescue [1], [2], owing to their high agility and mechanical simplicity [3]. However, quadrotors are underactuated, strongly coupled, and highly nonlinear systems whose dynamics become particularly challenging during aggressive maneuvers involving large-angle rotations and rapid trajectory transitions [4], [5]. Achieving accurate and stable trajectory tracking under such demanding conditions remains a fundamental challenge in UAV control [4], [5]. Moreover, practical UAV systems operate on onboard digital processors, where control algorithms are inherently executed in discrete time. Consequently, finite sampling intervals may become non-negligible relative to system dynamics under practical computational and communication constraints [6], [7].

Geometric control formulations on the Special Orthogonal Group (SO(3)) provide a global and singularity-free representation of rigid-body attitude, thereby avoiding limitations associated with traditional Euler-angle and quaternion-based methods [8], [5]. Such formulations have demonstrated strong performance in aggressive UAV maneuvers [4], [5]. When combined with recursive backstepping structures, geometric control becomes particularly attractive for quadrotor trajectory tracking. Backstepping provides a systematic Lyapunov-based framework for handling nonlinear coupling and underactuated dynamics [9], [4]. Nevertheless, most geometric backstepping approaches for quadrotor systems remain predominantly formulated in the continuous-time (CT) domain [4], [10].

In practical implementations, CT controllers are commonly deployed through sampled-data execution using emulation-based discretization [6]. Existing studies have investigated Lyapunov-based redesign strategies for sampled implementations by modifying CT controllers to compensate for sampling effects [11]. Such implementations typically assume sufficiently high sampling rates, which may not always be achievable under practical computational or communication limitations [6]. Under non-negligible sampling effects, finite-step dynamics may alter closed-loop behavior and stability properties [7], [12]. In particular, a negative CT Lyapunov derivative $\dot{V} < 0$ does not necessarily imply a negative discrete-time (DT) Lyapunov difference $\Delta V < 0$ [6], [7], [12]. Consequently, Lyapunov stability properties predicted by CT analysis may not directly translate into sampled implementations. Such discrepancies motivate the development of direct DT controller formulations that explicitly account for finite-step effects [13], [14], [12].

To explicitly account for finite-step effects during controller synthesis, direct DT controller formulations provide a natural alternative [6], [7]. Among nonlinear design approaches, backstepping remains attractive due to its recursive structure and systematic Lyapunov construction [15], [13]. However, extending geometric backstepping directly into the DT domain introduces several fundamental challenges. Within DT backstepping, future virtual control

[1]C. Yuan and A. Rizzo are with the Department of Electrical, Electronics and Telecommunications Engineering, Politecnico di Torino, Turin, Italy. yuan.cao@polito.it; alessandro.rizzo@polito.it

laws naturally introduce noncausal dependencies [15]. Moreover, when attitude dynamics evolve on $\mathsf{SO}(3)$, prediction mechanisms must preserve the manifold structure to avoid violating geometric constraints [16], [17]. In addition, nested nonlinear difference equations can rapidly increase algebraic complexity [18], [19]. Establishing Lyapunov stability directly in the discrete domain also remains challenging [13], [14], [20], [7].

To address these challenges, this paper develops an intrinsic DT geometric backstepping framework for quadrotor trajectory tracking using structure-preserving SO(3) dynamics and a causal geometric prediction mechanism. The proposed framework resolves the noncausal dependence of DT backstepping through a geometric predictor, enabling causal one-step matching directly on $\mathsf{SO}(3)$. The Lie-group formulation preserves geometric consistency on $\mathsf{SO}(3)$. A DT Lyapunov difference analysis further characterizes sampling-dependent stability properties arising from finite-step residual effects.

The main contributions of this paper are summarized as follows:

- An intrinsic DT geometric backstepping framework is developed for aggressive quadrotor trajectory tracking under sampled implementation.
- A structure-preserving geometric predictor is proposed to resolve noncausal dependencies and enable causal one-step matching directly on $\mathsf{SO}(3)$.
- A DT Lyapunov characterization is established to explicitly capture finite-step residual effects and quantify sampling-dependent stability properties. These include residual scaling behavior and the evolution of the ultimate bound under varying sampling conditions.
- Extensive simulations under aggressive trajectories, large-angle maneuvers, and sampling-period variations validate the proposed framework and demonstrate behavior consistent with theoretical predictions.

The remainder of this paper is organized as follows. Section II reviews related work on geometric and DT quadrotor control. Section III introduces the mathematical preliminaries, structure-preserving DT modeling, and the geometric prediction mechanism. Sections IV and V present the DT backstepping designs for the translational and rotational subsystems together with their respective Lyapunov stability analyses. Simulation results are provided in Section VI, followed by concluding remarks in Section VII.

II. Related Work

This section reviews existing studies related to geometric backstepping control for quadrotor systems, sampled implementation of CT controllers, and challenges arising in direct DT formulations.

A. Geometric Backstepping Control for Quadrotors

Various nonlinear control strategies, including sliding mode control [21], feedback linearization [22], and model reference adaptive control [23], have been applied to quadrotor systems to address nonlinear dynamics and strong coupling effects. Among these approaches, backstepping has attracted considerable attention owing to its recursive structure and systematic Lyapunov-based design philosophy [13], [24], [4].

To improve performance under aggressive maneuvers involving large-angle attitude evolution, geometric formulations directly developed on $\mathsf{SO}(3)$ have been increasingly incorporated into backstepping-based UAV control designs [5], [4], [25]. Such formulations avoid singularities associated with local attitude parameterizations and preserve the intrinsic geometric structure of rotational dynamics. However, most existing geometric backstepping methods for quadrotor systems remain formulated in the CT domain [4], [10].

B. Sampled Implementation of CT Controllers

Practical UAV systems execute control algorithms on digital processors, where CT controllers are commonly implemented through sampled-data emulation [6]. Such approaches generally rely on sufficiently high sampling rates so that sampled implementations closely approximate the original CT behavior. However, under finite sampling intervals, discretization effects may alter closed-loop dynamics and degrade stability or performance [7], [12]. In particular, Lyapunov stability properties established in CT analysis do not necessarily remain valid after sampled implementation [13], [7]. Such discrepancies may become more pronounced during aggressive UAV maneuvers, where rapid state variations can increase sensitivity to finite-step effects. These limitations have motivated increasing interest in direct DT formulations that explicitly account for finite-step effects during controller synthesis.

C. Challenges in Direct DT Geometric Backstepping

Direct DT backstepping provides a systematic framework for sampled-data control design but introduces several fundamental challenges. Within DT backstepping, future virtual control laws naturally introduce noncausal dependencies because control inputs at the current step may require future states or virtual signals unavailable at the current sampling instant [15], [26]. In addition, repeated substitution of nonlinear difference equations can significantly increase algebraic complexity [18], [19]. Stability analysis is further complicated by cross terms and finite-step residual effects arising in the DT Lyapunov difference formulation [19], [27].

These challenges become more pronounced when attitude dynamics evolve on $\mathsf{SO}(3)$. Existing prediction or approximation approaches are typically developed in Euclidean spaces and may not preserve geometric constraints during DT evolution. Consequently, maintaining structure-preserving implementation directly on $\mathsf{SO}(3)$ remains challenging [16], [17].

D. Positioning of This Work

Despite these developments, existing studies on sampled-data nonlinear UAV control have primarily focused on individual aspects of the problem. CT backstepping approaches

mainly emphasize nonlinear tracking performance, while sampled implementations are commonly handled through emulation-based discretization, where finite-step sampled dynamics are not explicitly incorporated during controller synthesis. Existing direct DT formulations, on the other hand, rarely address geometric structure preservation and causality issues simultaneously on $\mathsf{SO}(3)$. Consequently, a unified DT geometric backstepping framework that simultaneously addresses finite-step sampled dynamics, causal DT implementation, and structure-preserving evolution on $\mathsf{SO}(3)$ remains relatively underexplored in the current literature. From this perspective, the present work is positioned within the emerging direction of intrinsic DT geometric control, where sampled implementation, finite-step Lyapunov evolution, and geometric consistency on $\mathsf{SO}(3)$ are treated within a unified framework.

III. Mathematical Preliminaries and DT Modeling

A. Geometric Notation and Properties on $\mathsf{SO}(3)$

1) Hat/Vee Operators and Basic Identities: To provide the mathematical foundation for the geometric controller design, the configuration space of the quadrotor attitude is modeled as the Special Orthogonal Group $\mathsf{SO}(3)$, defined as

$$\mathsf{SO}(3) = \{\mathbf{R} \in \mathbb{R}^{3\times 3} \mid \mathbf{R}^\top \mathbf{R} = \mathbf{I},\ \det(\mathbf{R}) = 1\}. \tag{1}$$

The Lie algebra associated with $\mathsf{SO}(3)$ is denoted by $\mathfrak{so}(3)$, which consists of all 3×3 skew-symmetric matrices [5].

The hat map $(\cdot)^\wedge : \mathbb{R}^3 \to \mathfrak{so}(3)$ establishes an isomorphism between a vector $\mathbf{x} = [x_1, x_2, x_3]^\top \in \mathbb{R}^3$ and a skew-symmetric matrix:

$$\mathbf{x}^\wedge = \begin{bmatrix} 0 & -x_3 & x_2 \\ x_3 & 0 & -x_1 \\ -x_2 & x_1 & 0 \end{bmatrix}. \tag{2}$$

The inverse map is denoted by the vee operator $(\cdot)^\vee : \mathfrak{so}(3) \to \mathbb{R}^3$, satisfying $(\mathbf{x}^\wedge)^\vee = \mathbf{x}$.

For any $\mathbf{x}, \mathbf{y} \in \mathbb{R}^3$, the following identity holds:

$$\mathbf{x}^\wedge \mathbf{y} = \mathbf{x} \times \mathbf{y}. \tag{3}$$

2) Exponential and Logarithmic Maps: A crucial operation in geometric control is the exponential map

$$\exp : \mathfrak{so}(3) \to \mathsf{SO}(3),$$

which maps elements from the tangent space to the manifold. For a vector $\boldsymbol{\phi} \in \mathbb{R}^3$, Rodrigues' formula gives the closed-form expression

$$\begin{aligned} \exp(\boldsymbol{\phi}^\wedge) = \mathbf{I} &+ \frac{\sin\|\boldsymbol{\phi}\|}{\|\boldsymbol{\phi}\|}\boldsymbol{\phi}^\wedge \\ &+ \frac{1-\cos\|\boldsymbol{\phi}\|}{\|\boldsymbol{\phi}\|^2}(\boldsymbol{\phi}^\wedge)^2. \end{aligned} \tag{4}$$

The logarithmic map

$$\log : \mathsf{SO}(3) \to \mathfrak{so}(3),$$

denotes the matrix logarithm on $\mathsf{SO}(3)$ and is given by

$$\log(\mathbf{R}) = \frac{\theta}{2\sin\theta}(\mathbf{R} - \mathbf{R}^\top), \tag{5}$$

where

$$\theta = \cos^{-1}\left(\frac{\mathrm{tr}(\mathbf{R}) - 1}{2}\right), \tag{6}$$

with the limit $\log(\mathbf{R}) \to 0$ as $\theta \to 0$.

3) Structure-Preserving Property: For any $\mathbf{R}_k \in \mathsf{SO}(3)$ and body angular velocity $\boldsymbol{\Omega}_k \in \mathbb{R}^3$, the update rule

$$\mathbf{R}_{k+1} = \mathbf{R}_k \exp\big(T_s \boldsymbol{\Omega}_k^\wedge\big) \tag{7}$$

guarantees that $\mathbf{R}_{k+1} \in \mathsf{SO}(3)$, i.e.,

$$\mathbf{R}_{k+1}^\top \mathbf{R}_{k+1} = \mathbf{I}.$$

This property is fundamental for avoiding numerical drift and preserving geometric consistency. In contrast, additive updates such as

$$\mathbf{R}_{k+1} \approx \mathbf{R}_k + \dot{\mathbf{R}}_k T_s \tag{8}$$

do not, in general, preserve the orthogonality constraint $\mathbf{R}^\top\mathbf{R} = \mathbf{I}$, and may lead to deviations from the manifold $\mathsf{SO}(3)$ over time [16], [28].

4) Attitude Error Representation and Useful Identities: For any $\mathbf{R} \in \mathsf{SO}(3)$ and $\mathbf{x} \in \mathbb{R}^3$, the identity

$$\mathbf{R}\mathbf{x}^\wedge\mathbf{R}^\top = (\mathbf{R}\mathbf{x})^\wedge \tag{9}$$

holds, which will be used repeatedly in the subsequent geometric derivations.

Define the attitude tracking error as

$$\mathbf{R}_e = \mathbf{R}_d^\top \mathbf{R}.$$

The attitude error function is defined as

$$\Psi(\mathbf{R}_e) = \frac{1}{2}\,\mathrm{tr}(\mathbf{I} - \mathbf{R}_e), \tag{10}$$

which satisfies $0 \le \Psi(\mathbf{R}_e) \le 2$ and achieves its global minimum at $\mathbf{R}_e = \mathbf{I}$. The function $\Psi(\mathbf{R}_e)$ is positive definite with respect to $\mathbf{R}_e = \mathbf{I}$.

The corresponding attitude error vector is defined as

$$\mathbf{e}_R = \frac{1}{2}(\mathbf{R}_e - \mathbf{R}_e^\top)^\vee. \tag{11}$$

a) Key Lemma: For any $\mathbf{R} \in \mathsf{SO}(3)$ and $\mathbf{a} \in \mathbb{R}^3$, let $\mathbf{A} = \mathbf{a}^\wedge$. Then

$$\big(\mathbf{R}\mathbf{A} + \mathbf{A}\mathbf{R}^\top\big)^\vee = \big(\mathrm{tr}(\mathbf{R})\mathbf{I} - \mathbf{R}\big)\mathbf{a}. \tag{12}$$

Define the matrix-valued function

$$\mathbf{D}(\mathbf{R}) = \frac{1}{2}\big(\mathrm{tr}(\mathbf{R})\mathbf{I} - \mathbf{R}\big), \tag{13}$$

which relates angular velocity errors to attitude error dynamics and will be used extensively in the controller design.

B. CT Quadrotor Dynamics

The quadrotor UAV is modeled as a rigid body evolving on the configuration manifold $SE(3) = \mathbb{R}^3 \times \mathsf{SO}(3)$. Let $\mathbf{p}, \mathbf{v} \in \mathbb{R}^3$ denote the position and velocity, $\mathbf{R} \in \mathsf{SO}(3)$ the attitude, and $\boldsymbol{\Omega} \in \mathbb{R}^3$ the angular velocity.

1) CT Dynamics on $SE(3)$: Under the rigid-body assumption with constant symmetric positive-definite inertia matrix $\mathbf{J}$, the Newton–Euler equations governing the system dynamics are

$$\dot{\mathbf{p}} = \mathbf{v}, \tag{14}$$

$$\dot{\mathbf{v}} = \frac{f}{m}\mathbf{R}\mathbf{e}_3 - g\mathbf{e}_3, \tag{15}$$

$$\dot{\mathbf{R}} = \mathbf{R}\boldsymbol{\Omega}^{\wedge}, \tag{16}$$

$$\mathbf{J}\dot{\boldsymbol{\Omega}} = -\boldsymbol{\Omega} \times (\mathbf{J}\boldsymbol{\Omega}) + \boldsymbol{\tau}. \tag{17}$$

Given a smooth desired position trajectory $\mathbf{p}_d(t)$ with specified yaw angle $\psi_d(t)$, the desired thrust vector is

$$\mathbf{F}_d = m(g\mathbf{e}_3 - \ddot{\mathbf{p}}_d). \tag{18}$$

Assuming non-zero thrust, the desired body z-axis is

$$\mathbf{b}_{3d} = \frac{\mathbf{F}_d}{\|\mathbf{F}_d\|}, \tag{19}$$

from which the desired rotation matrix $\mathbf{R}_d$ is constructed geometrically [5]. The desired angular velocity satisfies $\dot{\mathbf{R}}_d = \mathbf{R}_d\boldsymbol{\Omega}_d^{\wedge}$.

2) Tracking Error Dynamics: The position and velocity errors are

$$\mathbf{e}_p = \mathbf{p} - \mathbf{p}_d, \qquad \mathbf{e}_v = \mathbf{v} - \dot{\mathbf{p}}_d.$$

With attitude and angular velocity errors

$$\mathbf{e}_R = \frac{1}{2}(\mathbf{R}_e - \mathbf{R}_e^{\top})^{\vee}, \tag{20}$$

$$\mathbf{e}_\Omega = \boldsymbol{\Omega} - \mathbf{R}_e^{\top}\boldsymbol{\Omega}_d. \tag{21}$$

The time evolution of the attitude error vector satisfies

$$\dot{\mathbf{e}}_R = \mathbf{D}(\mathbf{R}_e)\mathbf{e}_\Omega, \tag{22}$$

where $\mathbf{D}(\cdot)$ is defined in Section II-A.

C. Structure-Preserving Discrete-Time Modeling

To enable digital implementation while preserving the geometric structure of $\mathsf{SO}(3)$, a structure-preserving discretization is adopted. Let the sampling period be $T_s > 0$ and define the discrete step k such that $t_k = kT_s$.

Unlike standard discretization methods that treat the state space as Euclidean, we employ a Lie group integration approach. This model serves two crucial purposes. First, it ensures structure preservation by guaranteeing $\mathbf{R}(k+1) \in \mathsf{SO}(3)$ inherently without requiring re-normalization. Second, it resolves causality issues by acting as a geometric predictor to compute the future attitude $\mathbf{R}(k+1)$ based on current information, addressing the noncausal problem often encountered in DT backstepping design.

1) Translational Dynamics: Since the position space $\mathbb{R}^3$ is Euclidean, a standard forward Euler discretization is sufficient:

$$\mathbf{p}(k+1) = \mathbf{p}(k) + T_s\mathbf{v}(k), \tag{23}$$

$$\mathbf{v}(k+1) = \mathbf{v}(k) + T_s\left(\frac{f(k)}{m}\mathbf{R}(k)\mathbf{e}_3 - g\mathbf{e}_3\right). \tag{24}$$

2) Rotational Dynamics (Geometric Predictor): For the attitude kinematics $\dot{\mathbf{R}} = \mathbf{R}\boldsymbol{\Omega}^{\wedge}$, the exact discretization on the manifold is used:

$$\mathbf{R}(k+1) = \mathbf{R}(k)\exp\big(T_s\boldsymbol{\Omega}(k)^{\wedge}\big). \tag{25}$$

For the angular velocity, a first-order forward Euler approximation is applied:

$$\boldsymbol{\Omega}(k+1) = \boldsymbol{\Omega}(k) + T_s\mathbf{J}^{-1}\big(\boldsymbol{\tau}(k) - \boldsymbol{\Omega}(k) \times (\mathbf{J}\boldsymbol{\Omega}(k))\big). \tag{26}$$

3) DT Desired Dynamics: The desired rotation evolves as

$$\mathbf{R}_d(k+1) = \mathbf{R}_d(k)\exp\big(T_s\boldsymbol{\Omega}_d(k)^{\wedge}\big). \tag{27}$$

The desired angular velocity is approximated by

$$\boldsymbol{\Omega}_d(k) \approx \frac{1}{T_s}\big(\log(\mathbf{R}_d(k-1)^{\top}\mathbf{R}_d(k))\big)^{\vee}. \tag{28}$$

4) DT Error Dynamics: Let $\mathbf{R}_e(k) = \mathbf{R}_d(k)^{\top}\mathbf{R}(k)$. The error propagation on the manifold is

$$\mathbf{R}_e(k+1) = \exp\big(-T_s\boldsymbol{\Omega}_d(k)^{\wedge}\big)\mathbf{R}_e(k)\exp\big(T_s\boldsymbol{\Omega}(k)^{\wedge}\big). \tag{29}$$

Define the error vectors

$$\mathbf{e}_R(k) = \frac{1}{2}(\mathbf{R}_e(k) - \mathbf{R}_e(k)^{\top})^{\vee}, \tag{30}$$

$$\mathbf{e}_\Omega(k) = \boldsymbol{\Omega}(k) - \mathbf{R}_e(k)^{\top}\boldsymbol{\Omega}_d(k). \tag{31}$$

A first-order error dynamics approximation used for Lyapunov design is given by

$$\mathbf{e}_R(k+1) = \mathbf{e}_R(k) + T_s\mathbf{D}(\mathbf{R}_e(k))\mathbf{e}_\Omega(k), \tag{32}$$

which is a first-order consistent DT approximation of $\dot{\mathbf{e}}_R = \mathbf{D}(\mathbf{R}_e)\mathbf{e}_\Omega$.

IV. Discrete-Time Translational Backstepping Controller

This section develops the outer-loop DT translational controller. The objective is to construct the thrust vector $\mathbf{F}_d(k)$ such that the vehicle position $\mathbf{p}(k)$ tracks the reference trajectory $\mathbf{p}_d(k)$. The controller is designed via a two-layer DT Lyapunov backstepping procedure with one-step exact matching and is fully consistent with the $\mathsf{SO}(3)$ rotational subsystem presented in the subsequent section.

A. Error Definitions and Discrete-Time Propagation

Define the position tracking error as

$$\mathbf{e}_p(k) = \mathbf{p}(k) - \mathbf{p}_d(k). \tag{33}$$

Based on the structure-preserving predictor, the DT position dynamics satisfy

$$\mathbf{p}(k+1) = \mathbf{p}(k) + T_s\mathbf{v}(k), \tag{34}$$

which implies the error propagation

$$\mathbf{e}_p(k+1) = \mathbf{e}_p(k) + T_s\left(\mathbf{v}(k) - \mathbf{v}_d(k)\right), \tag{35}$$

$$\mathbf{v}_d(k) = \frac{\mathbf{p}_d(k+1) - \mathbf{p}_d(k)}{T_s}, \tag{36}$$

where $T_s > 0$ denotes the sampling period.

The control objective is to construct a thrust input $\mathbf{F}_d(k)$ such that the translational error state

$$\mathbf{z}_T(k) = \begin{bmatrix}\mathbf{e}_p(k)\\ \mathbf{e}_v(k)\end{bmatrix}$$

converges to the origin.

B. Main Result: Control Law and Stability Guarantee

The main result is summarized below.

Theorem 1 (Global Exponential Stability of Translational Errors)**.** *Consider the DT translational error dynamics under the assumption that the reference trajectory $\mathbf{p}_d(t)$ is available with finite two-step preview.*

Let the desired thrust vector be designed as

$$\mathbf{F}_d(k) = m\left(g\mathbf{e}_3 + \frac{\mathbf{v}_v(k+1) - \mathbf{v}(k)}{T_s}\right), \tag{37}$$

where $\mathbf{v}_v(k{+}1)$ is a feasible one-step-ahead virtual velocity computed from the desired trajectory together with current state measurements.

Assume

$$K_p = K_p^\top \succ 0, \qquad \rho(I - K_pT_s) < 1.$$

Then there exists a positive constant $\bar{c}_T > 0$ such that

$$\Delta V_T(k) \le -\bar{c}_T\|\mathbf{z}_T(k)\|^2. \tag{38}$$

Consequently, the equilibrium $\mathbf{z}_T = 0$ of the DT translational subsystem is nominally globally exponentially stable.

For completeness, detailed derivations of the Lyapunov forward difference are provided in Appendix A.

Remark 1 (Implementability)**.** *The control law* (37) *involves a one-step-ahead virtual velocity $\mathbf{v}_v(k+1)$, which may introduce noncausal dependence in standard DT backstepping formulations.*

In the proposed implementation, this term is computed causally from the desired trajectory together with current state measurements.

A feasible realization is

$$\mathbf{v}_v(k+1) = \frac{\mathbf{p}_d(k+2) - \mathbf{p}(k+1) + (I - K_pT_s)\mathbf{e}_p(k+1)}{T_s}, \tag{39}$$

where

$$\mathbf{p}(k+1) = \mathbf{p}(k) + T_s\mathbf{v}(k),$$

and

$$\mathbf{e}_p(k+1) = \mathbf{p}(k+1) - \mathbf{p}_d(k+1).$$

Proof of Theorem 1.

First-layer backstepping design (position loop):

Consider the Lyapunov function

$$V_P(k) = \frac{1}{2}\|\mathbf{e}_p(k)\|^2. \tag{40}$$

Impose the one-step contraction model

$$\mathbf{e}_p(k+1) = (I - K_pT_s)\mathbf{e}_p(k), \tag{41}$$

which yields the virtual reference velocity

$$\mathbf{v}_v(k) = \frac{\mathbf{p}_d(k+1) - \mathbf{p}(k) + (I - K_pT_s)\mathbf{e}_p(k)}{T_s}. \tag{42}$$

Define

$$\mathbf{e}_v(k) = \mathbf{v}(k) - \mathbf{v}_v(k), \tag{43}$$

which gives

$$\mathbf{e}_p(k+1) = (I - K_pT_s)\mathbf{e}_p(k) + T_s\mathbf{e}_v(k). \tag{44}$$

Second-layer Lyapunov analysis:

Define the composite Lyapunov function

$$V_T(k) = \frac{1}{2}\|\mathbf{e}_p(k)\|^2 + \frac{1}{2}\|\mathbf{e}_v(k)\|^2. \tag{45}$$

The forward difference satisfies

$$\Delta V_T(k) = W_T(k) + \frac{1}{2}\|\mathbf{e}_v(k+1)\|^2, \tag{46}$$

where $W_T(k)$ collects the quadratic terms in $\mathbf{e}_p(k)$ and $\mathbf{e}_v(k)$.

Applying Young's inequality yields

$$W_T(k) \le -c_T\|\mathbf{z}_T(k)\|^2, \qquad c_T > 0, \tag{47}$$

where detailed coefficient expressions are given in Appendix A.

One-step exact matching:

The velocity dynamics satisfy

$$\mathbf{v}(k+1) = \mathbf{v}(k) + T_s\left(\frac{1}{m}\mathbf{F}_d(k) - g\mathbf{e}_3\right). \tag{48}$$

Imposing

$$\mathbf{e}_v(k+1) = 0$$

eliminates the forward Lyapunov term and yields the thrust law (37). Consequently,

$$\Delta V_T(k) \le -\bar{c}_T\|\mathbf{z}_T(k)\|^2, \tag{49}$$

which establishes nominal global exponential stability. □

C. Desired Thrust and Attitude Generation

The thrust magnitude and desired body z-axis are computed as

$$f(k) = \|\mathbf{F}_d(k)\|, \qquad \mathbf{b}_{3d}(k) = \frac{\mathbf{F}_d(k)}{\|\mathbf{F}_d(k)\|}. \tag{50}$$

The desired rotation matrix $\mathbf{R}_d(k) \in \mathsf{SO}(3)$ is constructed such that the thrust axis aligns with $\mathbf{b}_{3d}(k)$ while satisfying the yaw command $\psi_d(k)$.

The command pair $(\mathbf{R}_d(k), f(k))$ is then passed to the DT $\mathsf{SO}(3)$ attitude backstepping controller.

V. Discrete-Time SO(3) Backstepping Controller

This section presents the inner-loop DT rotational controller on $\mathsf{SO}(3)$. Following the translational subsystem, the design adopts a two-layer Lyapunov-based backstepping structure with causal one-step matching.

The objective is to construct a causal torque law that guarantees Semi-Globally Uniformly Ultimately Bounded (SGUUB) of the rotational tracking errors under intrinsic DT modeling. Before presenting the detailed backstepping construction, we first summarize the resulting control law and the corresponding stability guarantee.

A. DT Rotational Dynamics and Error Definitions

Consider the structure-preserving DT rotational dynamics

$$\begin{cases} \mathbf{R}(k+1) = \mathbf{R}(k)\exp(T_s\boldsymbol{\Omega}(k)^\wedge) \\ \boldsymbol{\Omega}(k+1) = \boldsymbol{\Omega}(k) + T_s\mathbf{J}^{-1}[\boldsymbol{\tau}(k) - \boldsymbol{\Omega}(k)\times(\mathbf{J}\boldsymbol{\Omega}(k))], \end{cases} \tag{51}$$

where $\mathbf{R}(k) \in \mathsf{SO}(3)$, $\boldsymbol{\Omega}(k) \in \mathbb{R}^3$, and $\mathbf{J} \succ 0$.

Define the attitude error

$$\mathbf{R}_e(k) = \mathbf{R}_d^\top(k)\mathbf{R}(k), \tag{52}$$

and the corresponding attitude error vector

$$\mathbf{e}_R(k) = \tfrac{1}{2}\big(\mathbf{R}_e(k) - \mathbf{R}_e^\top(k)\big)^\vee. \tag{53}$$

Let the virtual angular velocity be chosen as

$$\boldsymbol{\Omega}_v(k) = \mathbf{R}_e^\top(k)\boldsymbol{\Omega}_d(k) - K_R\mathbf{e}_R(k), \qquad K_R > 0, \tag{54}$$

and define the angular velocity error

$$\mathbf{e}_\omega(k) = \boldsymbol{\Omega}(k) - \boldsymbol{\Omega}_v(k). \tag{55}$$

The control torque is designed via the one-step matching law

$$\boldsymbol{\tau}(k) = \mathbf{J}\frac{\boldsymbol{\Omega}_v(k+1) - \boldsymbol{\Omega}(k)}{T_s} + \boldsymbol{\Omega}(k)\times(\mathbf{J}\boldsymbol{\Omega}(k)). \tag{56}$$

Define the stacked rotational error state

$$\mathbf{z}_R(k) = \begin{bmatrix} \mathbf{e}_R(k) \\ \mathbf{e}_\omega(k) \end{bmatrix}. \tag{57}$$

B. Main Result: Control Law and Stability Guarantee

Theorem 2 (SGUUB Stability of Rotational Errors)**.** *Consider the DT rotational dynamics* (51) *with the error definitions* (52)–(55)*, and the control law* (56)*. Suppose that the sampling period satisfies*

$$T_s < 2\lambda_{\min}\left(\mathbf{K}_R^{1/2}\mathbf{J}\mathbf{K}_R^{1/2}\right),$$

and that the discretization residual satisfies

$$|r_R(k)| \le \delta_R, \qquad \delta_R = O(T_s^2).$$

Then there exists a constant $\bar{c}_R > 0$ such that the composite Lyapunov forward difference satisfies

$$\Delta V_\Omega(k) \le -\bar{c}_R\|\mathbf{z}_R(k)\|^2 + \delta_R, \tag{58}$$

where $\mathbf{z}_R(k)$ is defined in (57)*. Consequently, the rotational tracking errors are SGUUB, with an ultimate bound characterized by*

$$\mathcal{B}_R = \left\{\mathbf{z}_R :\ \|\mathbf{z}_R\| \le \sqrt{\delta_R/\bar{c}_R}\right\}.$$

The origin and bound of the residual term $r_R(k)$ are clarified in Appendix B.

Remark 2 (Residual Origin and Sampling-Dependent Bound)**.** *The residual $r_R(k)$ arises from higher-order $\mathcal{O}(T_s^2)$ terms in the DT Lyapunov difference on $\mathsf{SO}(3)$ due to the exponential map and Baker–Campbell–Hausdorff (BCH) expansion, and is intrinsic to the Lie-group structure.*

The desired angular velocity $\Omega_d(k)$ is obtained via finite-difference approximation of R_d, introducing an $\mathcal{O}(T_s)$ error, which contributes an $\mathcal{O}(T_s^2)$ term to the Lyapunov difference.

Both contributions scale as $\mathcal{O}(T_s^2)$ from distinct mechanisms (Lie-group discretization and reference approximation), and therefore do not alter the SGUUB property, but determine the ultimate bound.

In contrast, the translational subsystem admits an exact quadratic Lyapunov difference under one-step matching, and hence no discretization residual.

Since $\delta_R = O(T_s^2)$ and the residual contribution depends on the sampling period, smaller sampling periods generally lead to a smaller ultimate bound in Theorem 2. This dependence is further quantified and validated in the simulation section.

The reference approximation error is not separated, but absorbed into the unified residual bound δ_R, whose effect on the ultimate bound is quantified empirically through the sampling-dependent UUB radius in the simulation section.

Proof of Theorem 2.

Error propagation on $\mathsf{SO}(3)$:

The attitude error dynamics on the manifold satisfy

$$\mathbf{R}_e(k+1) = \exp(-T_s\boldsymbol{\Omega}_d(k)^\wedge)\,\mathbf{R}_e(k)\,\exp(T_s\boldsymbol{\Omega}(k)^\wedge). \tag{59}$$

Using the kinematic identity $\dot{\mathbf{e}}_R = \mathbf{D}(\mathbf{R}_e)\mathbf{e}_\Omega$ from Section II, a first-order consistent DT approximation yields

$$\mathbf{e}_R(k+1) = \mathbf{e}_R(k) + T_s\mathbf{D}(\mathbf{R}_e(k))\,\mathbf{e}_\Omega(k). \tag{60}$$

First-layer backstepping design (virtual angular velocity):

Consider the geometric potential function

$$V_R(k) = \tfrac{1}{2}\,\mathrm{tr}(\mathbf{I} - \mathbf{R}_e(k)). \tag{61}$$

Using a first-order expansion of the discrete error dynamics, the Lyapunov forward difference can be expressed as

$$\Delta V_R(k) = T_s\,\mathbf{e}_R^\top(k)\big(\boldsymbol{\Omega}(k) - \mathbf{R}_e^\top(k)\boldsymbol{\Omega}_d(k)\big) + r_R(k), \tag{62}$$

where $r_R(k) = \mathcal{O}(T_s^2)$ and is uniformly bounded on compact sets. Thus, $|r_R(k)| \le \delta_R$ with $\delta_R = \mathcal{O}(T_s^2)$. Substituting the virtual angular velocity yields

$$\Delta V_R(k) = -T_s\,\mathbf{e}_R^\top\mathbf{K}_R\mathbf{e}_R + T_s\,\mathbf{e}_R^\top\mathbf{e}_\omega + r_R(k). \tag{63}$$

Second-layer Lyapunov analysis (angular velocity loop): Define

$$V_\Omega(k) = V_R(k) + \tfrac{1}{2}\mathbf{e}_\omega^\top\mathbf{J}\mathbf{e}_\omega. \tag{64}$$

The Lyapunov difference admits the decomposition

$$\Delta V_\Omega(k) = W_\Omega(k) + \tfrac{1}{2}\mathbf{e}_\omega^\top(k+1)\mathbf{J}\mathbf{e}_\omega(k+1), \tag{65}$$

where

$$W_\Omega(k) = -T_s\,\mathbf{e}_R^\top\mathbf{K}_R\mathbf{e}_R + T_s\,\mathbf{e}_R^\top\mathbf{e}_\omega - \tfrac{1}{2}\mathbf{e}_\omega^\top\mathbf{J}\mathbf{e}_\omega + r_R(k). \tag{66}$$

Using the matrix form of Young's inequality, for any $\mathbf{A} \succ 0$,

$$T_s\mathbf{e}_R^\top\mathbf{e}_\omega \le \frac{T_s}{2}\mathbf{e}_R^\top\mathbf{A}\mathbf{e}_R + \frac{T_s}{2}\mathbf{e}_\omega^\top\mathbf{A}^{-1}\mathbf{e}_\omega,$$

which gives

$$\begin{aligned} W_\Omega(k) \le\ & -T_s\,\mathbf{e}_R^\top\Big(\mathbf{K}_R - \tfrac{1}{2}\mathbf{A}\Big)\mathbf{e}_R \\ & - \tfrac{1}{2}\mathbf{e}_\omega^\top\Big(\mathbf{J} - T_s\mathbf{A}^{-1}\Big)\mathbf{e}_\omega + r_R(k). \end{aligned}$$

Choose $\mathbf{A} = \beta\mathbf{K}_R$, with $0 < \beta < 2$. Then

$$\mathbf{K}_R - \tfrac{1}{2}\mathbf{A} = \Big(1 - \tfrac{\beta}{2}\Big)\,\mathbf{K}_R \succ 0,$$

and the second quadratic term is negative definite if

$$\mathbf{J} - \frac{T_s}{\beta}\mathbf{K}_R^{-1} \succ 0.$$

Equivalently,

$$T_s < \beta\lambda_{\min}\left(\mathbf{K}_R^{1/2}\mathbf{J}\mathbf{K}_R^{1/2}\right).$$

Letting $\beta \to 2^-$, this condition is guaranteed whenever

$$T_s < 2\lambda_{\min}\left(\mathbf{K}_R^{1/2}\mathbf{J}\mathbf{K}_R^{1/2}\right). \tag{67}$$

For diagonal $\mathbf{K}_R$ and $\mathbf{J}$, the above condition reduces to

$$T_s < 2\min_i K_{R,i}J_i. \tag{68}$$

Hence there exists $\bar{c}_R > 0$ such that

$$W_\Omega(k) \le -\bar{c}_R\|\mathbf{z}_R(k)\|^2 + \delta_R.$$

Under the one-step matching condition $\mathbf{e}_\omega(k+1) = 0$, this yields

$$\Delta V_\Omega(k) \le -\bar{c}_R\|\mathbf{z}_R(k)\|^2 + \delta_R,$$

which proves Theorem 2. *One-step exact matching:* Imposing the one-step exact matching condition

$$\mathbf{e}_\omega(k+1) = 0$$

eliminates the forward Lyapunov term and yields the torque control law (56).

Causal computation of future virtual rate: The future virtual angular velocity $\boldsymbol{\Omega}_v(k+1)$ is computed using the structure-preserving predictor

$$\boldsymbol{\Omega}_v(k+1) = \mathbf{R}_e^\top(k+1)\boldsymbol{\Omega}_d(k+1) - K_R\mathbf{e}_R(k+1), \tag{69}$$

where the predicted attitude is given by

$$\mathbf{R}(k+1) = \mathbf{R}(k)\exp(T_s\boldsymbol{\Omega}(k)^\wedge). \tag{70}$$

This establishes the claimed SGUUB stability result. □

VI. Simulation Results

This section evaluates the proposed intrinsic DT geometric backstepping framework through numerical simulations, with the primary objective of validating the sampling-consistent Lyapunov properties established in the theoretical analysis. The simulation environment and nominal parameters are first introduced, followed by tracking experiments under aggressive reference trajectories, including figure-8 and helical maneuvers, as well as a 360° flip to verify large-angle consistency on $\mathsf{SO}(3)$. Geometric consistency is then examined by analyzing the preservation of the rotation matrix orthogonality, confirming the structure-preserving property of the proposed formulation. Subsequently, the discrete-time Lyapunov behavior is investigated to verify the predicted dissipative property and the boundedness of sampling-induced residual dynamics. Finally, a sampling-sensitivity study is conducted to characterize the stability evolution with respect to the sampling period, including behavior near the theoretical limit, and is complemented by a comparison with an emulation-based baseline to highlight the structural inconsistency of continuous-time Lyapunov analysis under sampling.

A. Simulation Setup

1) Simulation Platform: The simulation environment is based on the MathWorks Quadcopter Project in MATLAB/Simulink, developed from the Parrot® mini-drone platform. The platform features a nonlinear quadrotor model that incorporates key physical effects, including sensor noise, actuator dynamics, and environmental disturbances. It serves as a medium-fidelity simulation model for control algorithm evaluation. The nominal physical parameters are: the mass $m = 0.063$ kg, gravitational acceleration $g = 9.8$ m/s^2, and the inertia matrix $\mathbf{J} = 10^{-4}\cdot\mathrm{diag}(0.5829,\, 0.7169,\, 1)$ kg$\cdot$m^2. All simulations use a fixed-step solver with sampling period $T_s = 0.005$ s (200 Hz), consistent with onboard digital implementation. The control gains are selected as $\mathbf{K}_p = \mathrm{diag}(0.2, 0.2, 0.2)$ and $\mathbf{K}_R = \mathrm{diag}(75, 60, 50)$. From the sampling condition (68), for the given inertia matrix $\mathbf{J}$, the bound evaluates to

$$T_s^{\max,\mathrm{th}} \approx 8.60\,\mathrm{ms}.$$

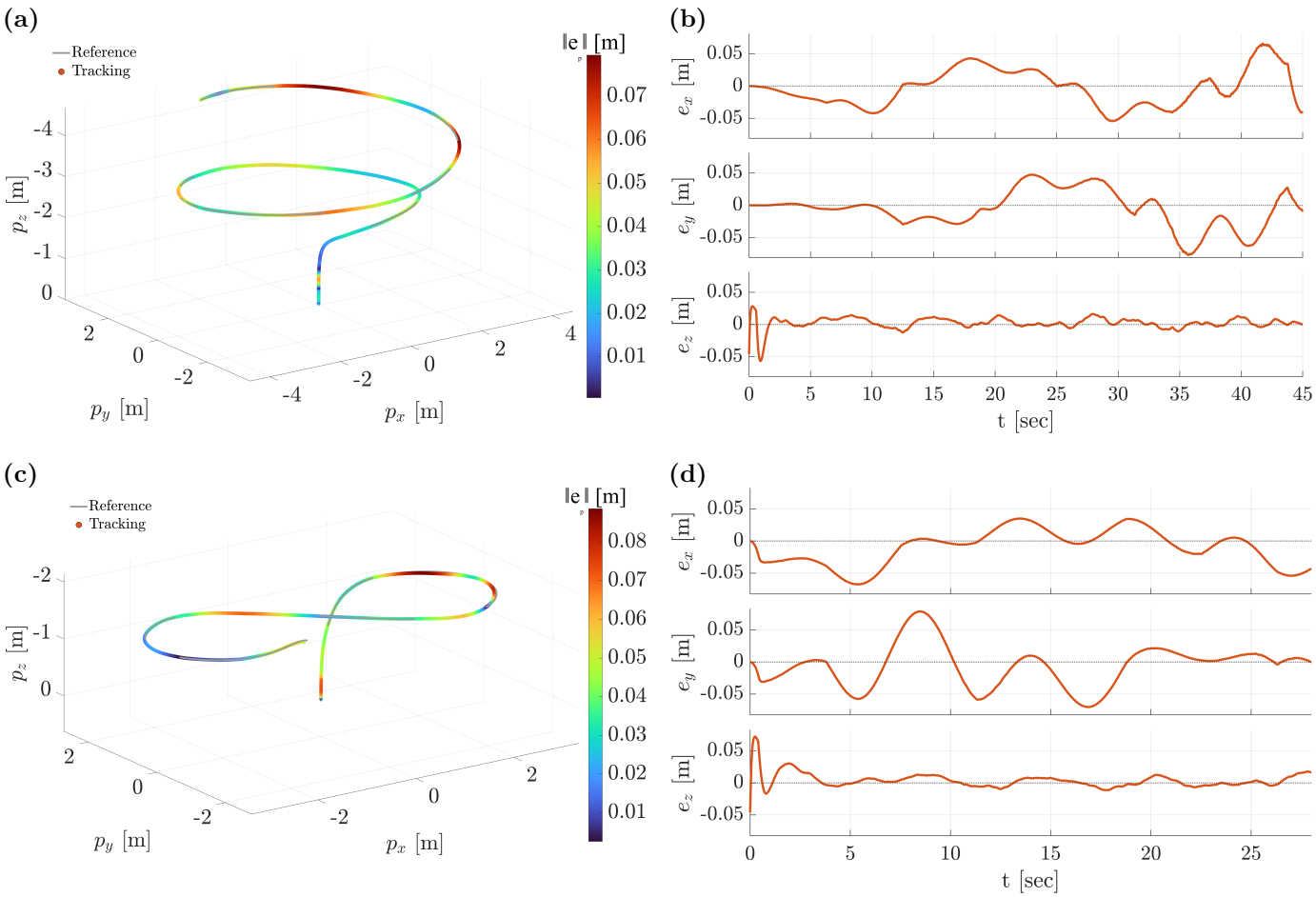


Fig. 1: Tracking performance under aggressive maneuvers. **(a)** Helical trajectory tracking. **(b)** Position errors for the helical maneuver. **(c)** Figure-8 trajectory tracking. **(d)** Position errors for the figure-8 maneuver.

The nominal sampling period $T_s = 5\,\text{ms}$ lies well within this admissible range.

2) Test Scenarios: To evaluate the proposed controller under demanding kinematic and dynamic conditions, minimum-snap trajectory generation is used to produce smooth reference signals with derivatives up to the fourth order. These trajectories intentionally drive the vehicle away from near-hover operating conditions in order to excite strong translational–rotational coupling. Two aggressive trajectory-tracking maneuvers are considered.

(1) A Figure-8 trajectory with lateral excursion ± 4 m at constant altitude 1.5 m, which introduces continuous curvature variation and coordinated banked turns.

(2) A spatial helical trajectory with lateral excursion ± 5 m and vertical variation from 1.5 m to 5.5 m, which generates sustained large tilt angles during aggressive flight.

In addition, a 360° flip maneuver is performed as a large-attitude rotation test to verify the singularity-free property and large-angle consistency of the $\mathsf{SO}(3)$ geometric formulation. During this maneuver, the outer-loop translational backstepping controller is temporarily disabled and a prescribed rotational trajectory is applied directly to the geometric attitude controller.

B. Performance under Aggressive and Large-Angle Maneuvers

The resulting three-dimensional trajectories for the helical and figure-8 maneuvers are shown in Fig. 1(a) and (c), respectively. The quadrotor accurately follows the commanded trajectories throughout the maneuver duration, including segments with rapid direction changes and altitude variations, indicating stable closed-loop behavior during aggressive flight.

The corresponding position tracking errors $\mathbf{e}_p = [e_x, e_y, e_z]^\top$ are reported in Fig. 1(b) and Fig. 1(d). The errors remain uniformly bounded and rapidly converge after short transient phases. The steady-state tracking error remains below approximately 0.06 m in the lateral directions and 0.04 m in the vertical direction, demonstrating high outer-loop tracking accuracy without drift or oscillatory growth during the entire maneuver.

Fig. 2 illustrates the vehicle orientation evolution along the flight trajectory during the maneuver. The vehicle executes the commanded flip maneuver smoothly while maintaining a coherent orientation evolution along the flight path.

For interpretability, Fig. 3(a) presents the attitude profile

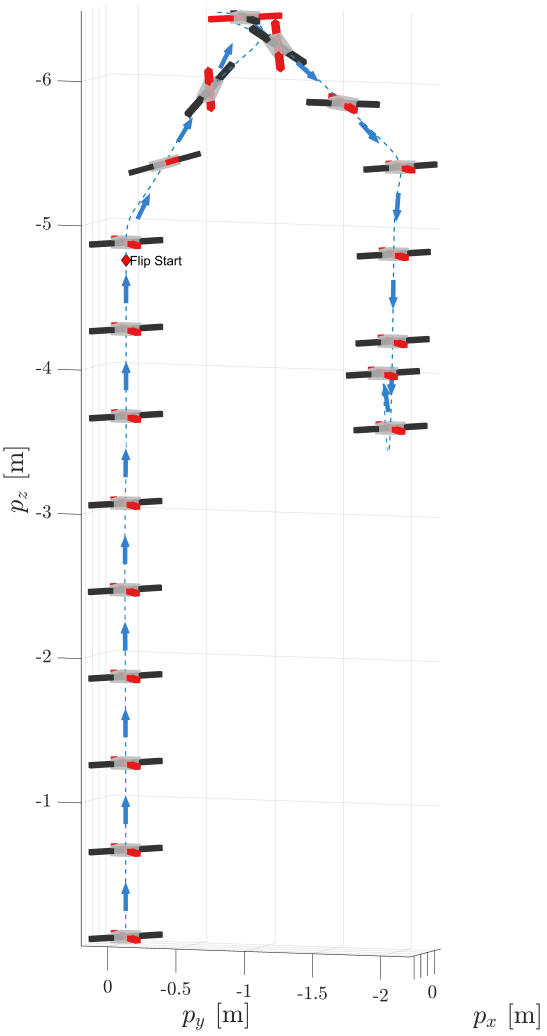


Fig. 2: Three-dimensional flight path with body snapshots illustrating the vehicle orientation evolution; the flip start is marked.

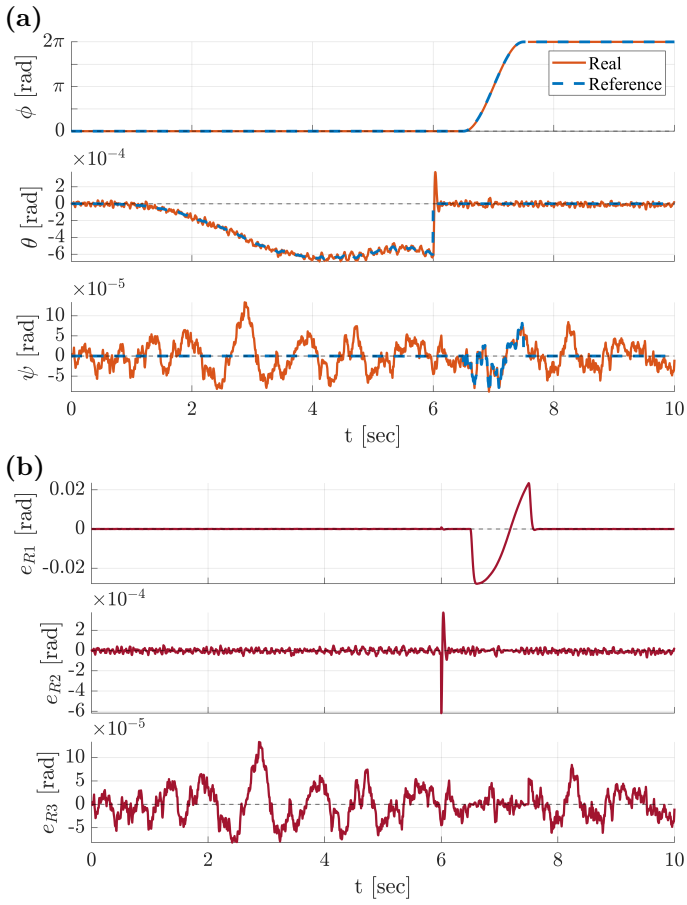


Fig. 3: Attitude tracking performance for the 360° flip maneuver. **(a)** Euler-angle representation of the attitude evolution (roll ϕ, pitch θ, yaw ψ), shown only for visualization; the tracked attitude closely follows the reference throughout the maneuver. **(b)** Geometric attitude error components $\mathbf{e}_R = [e_{R1}, e_{R2}, e_{R3}]^\top$, which remain bounded and rapidly return to a small neighborhood of the origin after the flip.

using Euler angles. Although Euler-angle representations are known to exhibit singularities and branch discontinuities, the attitude trajectories remain smooth throughout the 360° flip maneuver without numerical irregularities. This provides an intuitive illustration of the singularity-free property of the proposed $\mathsf{SO}(3)$ geometric controller.

More importantly, the intrinsic geometric attitude error $\mathbf{e}_R \in \mathbb{R}^3$, shown in Fig. 3(b), remains uniformly bounded during the maneuver and rapidly converges to a small residual set. This confirms that the controller maintains consistent tracking performance even under large-angle rotations, without relying on small-angle approximations.

These results confirm that the proposed DT geometric backstepping controller achieves accurate trajectory tracking under aggressive maneuvers while preserving smooth and singularity-free attitude behavior.

C. Lyapunov Consistency under Sampling Variations

This subsection establishes that the Lyapunov-based stability properties are consistently preserved in the discrete-time implementation under sampling variations. To evaluate the sampling-dependent behavior, the sampling period is varied over a wide range while keeping all controller gains fixed. The explored range spans the theoretically admissible region and approaches the predicted sampling limit $T_s^{\max,\mathrm{th}} \approx 8.6$ ms.

Geometric structure preservation. The proposed controller employs a structure-preserving Lie-group update in (25). To verify numerical consistency during aggressive maneuvers, the orthogonality error $\epsilon_R(k) = \|\mathbf{R}^\top(k)\mathbf{R}(k) - \mathbf{I}\|_F$ is monitored throughout the simulations.

As shown in Fig. 4, the error remains at machine precision, on the order of 10^{-16}, across all maneuvers, including the 360° flip. No drift accumulation is observed despite the high-angular-velocity phase, confirming that the proposed discrete-time formulation preserves the SO(3) structure without requiring re-projection or normalization. This structure preservation provides the foundation for the subsequent Lyapunov-based analysis in the discrete-time

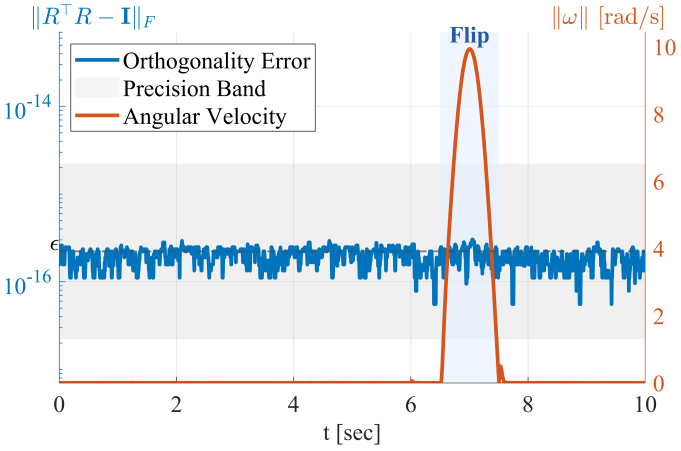


Fig. 4: Orthogonality error $\|R^\top R - I\|_F$ over time during the aggressive maneuver. The shaded band denotes the machine-precision band, and the dashed line indicates the numerical precision level ϵ. Even during the high-angular-velocity flip phase, highlighted region, the error remains within the machine-precision band, confirming that the proposed structure-preserving update maintains the SO(3) orthogonality without requiring re-normalization.

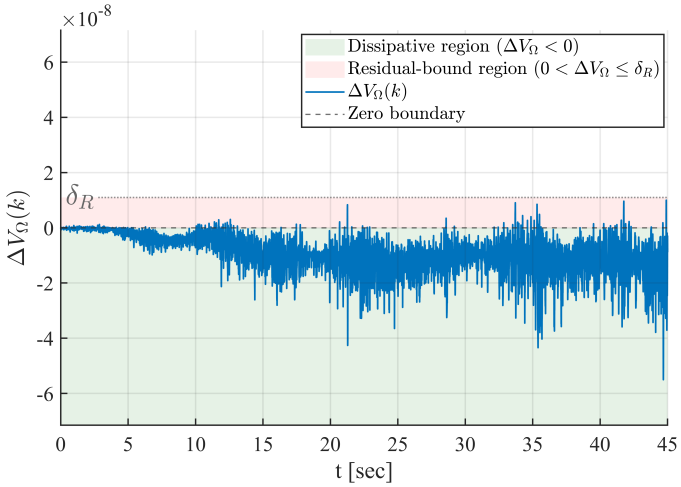


Fig. 5: DT Lyapunov forward difference $\Delta V_\Omega(k)$ during the aggressive helical maneuver. The shaded regions indicate the dissipative region ($\Delta V_\Omega < 0$) and the residual-bound region ($0 < \Delta V_\Omega \leq \delta_R$). The Lyapunov difference remains predominantly negative, while small positive excursions remain bounded by δ_R, validating the predicted $\mathcal{O}(T_s^2)$ discretization residual.

setting.

DT Lyapunov behavior. The dissipative behavior of the control law is evaluated through the DT Lyapunov forward difference $\Delta V_\Omega(k)$, which satisfies the bound in (58). Fig. 5 shows the evolution of $\Delta V_\Omega(k)$ during the aggressive helical maneuver.

The Lyapunov difference remains predominantly negative, confirming the dissipative property induced by the causal $\mathsf{SO}(3)$ predictor. Occasional positive excursions are observed but remain strictly bounded within δ_R, consistent with the theoretical $\mathcal{O}(T_s^2)$ discretization residual.

Sampling-induced Lyapunov residual scaling. To quantify the effect of sampling on the Lyapunov behavior, Fig. 6 shows the scaling of the positive Lyapunov residual $\Delta V_\Omega^+(k)$ as the sampling period increases. The maximum positive excursions scale approximately with T_s^2, consistent with the residual bound derived in Theorem 2. Moreover, the onset of nonzero residuals is aligned with the theoretical feasibility limit, confirming the predicted transition in the DT Lyapunov difference, where sampling-induced residuals give rise to occasional positive increments.

Empirical UUB radius under sampling. The impact of the sampling-induced residual on closed-loop stability is further illustrated in Fig. 7. The empirical ultimate bound $\hat{r}_B(T_s)$ is estimated from the steady-state magnitude of the composite rotational error $\|z_R\|$ after the transient phase.

As the sampling period increases, the empirical bound grows gradually, consistent with the increase of the Lyapunov residual. As T_s approaches the theoretical feasibility limit, the bound expands more rapidly, indicating a stronger influence of discretization effects on the closed-loop behavior.

This trend can be directly attributed to the sampling-induced residual δ_R, which becomes observable as small-scale fluctuations at the 10^{-8} level once the tracking error diminishes. These transient peaks are consistent with the analytical $\mathcal{O}(T_s^2)$ bound and reflect the UUB property of the closed-loop system established in Theorem 2.

These results demonstrate that the Lyapunov-based analysis not only guarantees stability but also quantitatively predicts the sampling-dependent evolution of the ultimate bound, linking the discretization residual, the invariant set $\mathcal{B}_R$, and the observed closed-loop behavior.

D. Comparison with Emulation-Based Discretization

This subsection compares the proposed direct DT controller with an emulation-based CT geometric backstepping baseline. The baseline follows the same CT design and is implemented digitally by sampling the corresponding control law (see Appendix C).

Lyapunov inconsistency under emulation. Fig. 8 compares the DT Lyapunov difference $\Delta V_\Omega(k)$ with the sampled continuous-time prediction $T_s \dot{V}_\Omega(k)$ at $T_s = 50$ ms, which lies well beyond the admissible sampling region of the proposed DT formulation. This choice intentionally places the system in a regime where instability occurs, allowing the validity of the Lyapunov prediction under emulation to be critically examined.

This is not observed. While $T_s \dot{V}_\Omega(k)$ remains predominantly negative, $\Delta V_\Omega(k)$ becomes positive after the onset of instability. Hence, $\dot{V}_\Omega < 0$ does not imply $\Delta V_\Omega(k) < 0$ in the sampled system, and the Lyapunov decrease mechanism is lost.

This behavior reflects a structural limitation under sampling, particularly in regimes where sampling effects are

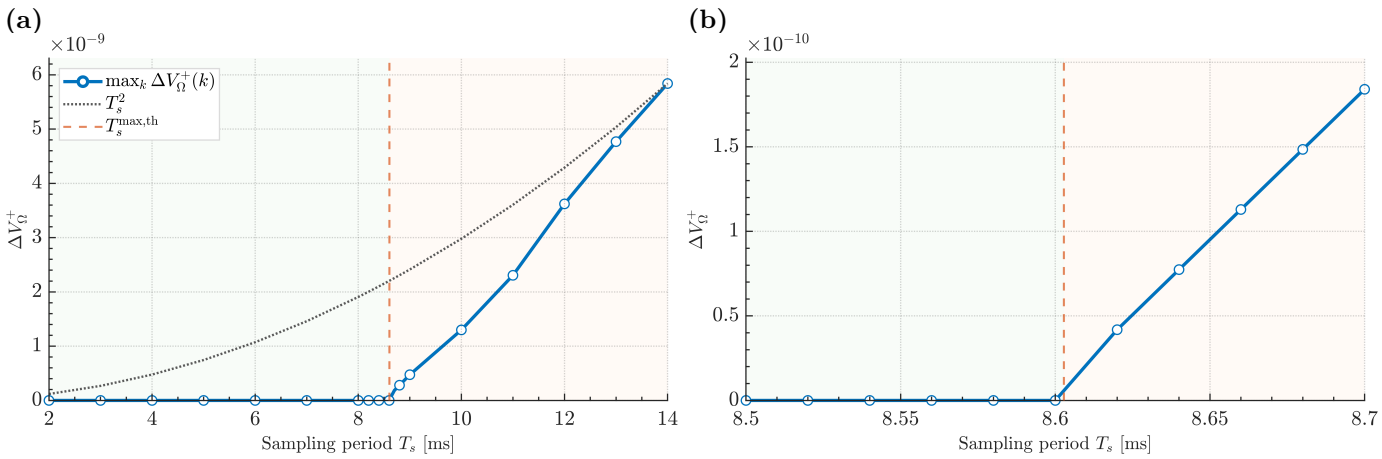


Fig. 6: Scaling of the positive Lyapunov residual with respect to the sampling period, measured by the maximum positive increment $\max \Delta V_\Omega^+(k)$. The dashed vertical line indicates the theoretical feasibility limit $T_s^{\max,\text{th}}$. **(a)** Global view showing $\max_k \Delta V_\Omega^+(k)$ together with a reference T_s^2 curve, highlighting the theory-consistent second-order scaling predicted by the DT analysis. **(b)** Zoomed view near $T_s^{\max,\text{th}}$, showing the local transition region where positive Lyapunov increments begin to emerge.

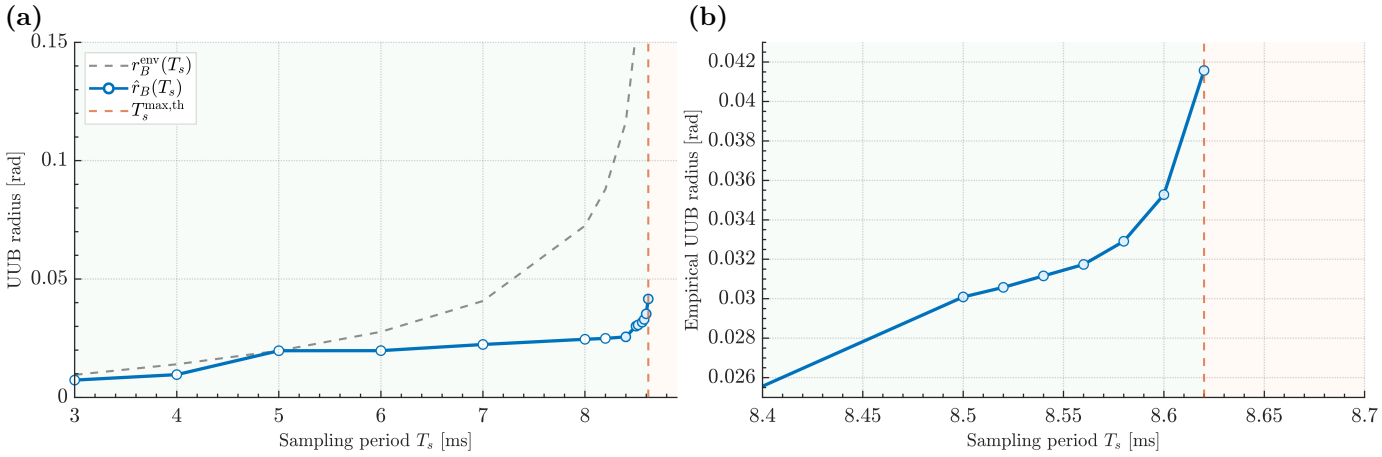


Fig. 7: Empirical ultimate bound of the rotational tracking error as a function of the sampling period. The blue curve shows the simulation-based estimate $\hat{r}_B(T_s)$, while the dashed curve represents the conservative Lyapunov-based envelope $r_B^{\text{env}}(T_s)$. The dashed vertical line indicates the theoretical feasibility limit $T_s^{\max,\text{th}}$. **(a)** Global view over the entire sampling range. **(b)** Zoomed view near the theoretical limit, highlighting the rapid growth of the empirical radius as T_s approaches $T_s^{\max,\text{th}}$.

non-negligible: the continuous-time Lyapunov framework does not explicitly account for sampling-induced dynamics and therefore may not characterize discrete-time Lyapunov evolution. Importantly, this mismatch persists even when the continuous-time Lyapunov prediction indicates a dissipative trend, revealing an inconsistency between analysis and implementation under sampling.

In contrast, the proposed direct DT formulation evaluates $\Delta V_\Omega(k)$ intrinsically in discrete time, preserving analysis–implementation consistency within the admissible sampling region (cf. Fig. 5).

Sampling-dependent closed-loop behavior.

Fig. 9 shows the post-transient error $\|z_R\|$ across sampling periods.

The proposed DT controller exhibits monotonic degradation with increasing T_s and remains bounded up to the theoretical sampling limit, providing a predictable sampling-dependent stability characterization.

The emulation-based controller does not. Stability is non-monotonic: for example, the response is stable at $T_s = 5$ ms and 8 ms, but unstable at 6 ms. Moreover, stability is not preserved across neighboring sampling periods, indicating the absence of local consistency with respect to T_s. Stability is therefore not an ordered function of T_s and cannot be inferred from $\dot{V}_\Omega$.

This irregularity is a direct consequence of Lyapunov inconsistency under sampling. Without modeling sampling-induced dynamics, the CT framework may not provide a valid and predictable stability characterization after discretization due to sampling-induced effects

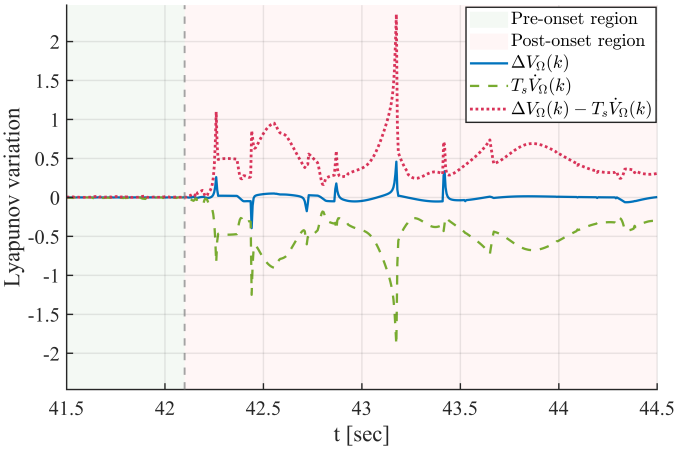


Fig. 8: Lyapunov inconsistency under emulation-based discretization. The discrete-time variation $\Delta V_\Omega(k)$ deviates from the sampled continuous-time prediction $T_s\dot{V}_\Omega(k)$, indicating loss of the Lyapunov decrease mechanism after sampling.

The proposed method preserves analysis–implementation consistency and yields a predictable sampling-dependent stability characterization. Emulation-based discretization may fail to provide a consistent characterization in the considered setting.

VII. Conclusion

This paper addressed a fundamental inconsistency arising in sampled implementations of geometric control systems, where CT Lyapunov conditions do not, in general, guarantee equivalent DT Lyapunov behavior under non-negligible sampling effects. To resolve this issue, an intrinsic DT geometric backstepping framework for quadrotor trajectory tracking on $\mathsf{SO}(3)$ was developed, ensuring that controller synthesis, Lyapunov analysis, and implementation are formulated within a unified DT framework.

Two complementary mechanisms were introduced to address the principal challenges of DT geometric backstepping. A structure-preserving Lie-group formulation maintains geometric evolution of the attitude dynamics directly on $\mathsf{SO}(3)$ throughout sampled operation, while a geometric predictor resolves the noncausal dependence inherent in DT backstepping by enabling causal one-step matching. Together, these components support a rigorous DT Lyapunov difference analysis establishing global exponential stability of the translational subsystem and SGUUB of the rotational tracking errors with sampling-dependent margins.

Simulation results under aggressive trajectory tracking, large-angle maneuvers, and sampling-period variations demonstrated accurate tracking performance, machine-precision preservation of $\mathsf{SO}(3)$ orthogonality, and sampling-dependent behavior consistent with theoretical predictions. In particular, the predicted residual scaling and invariant-set evolution were supported by numerical observations, supporting the use of intrinsic DT analysis for characterizing sampled closed-loop behavior.

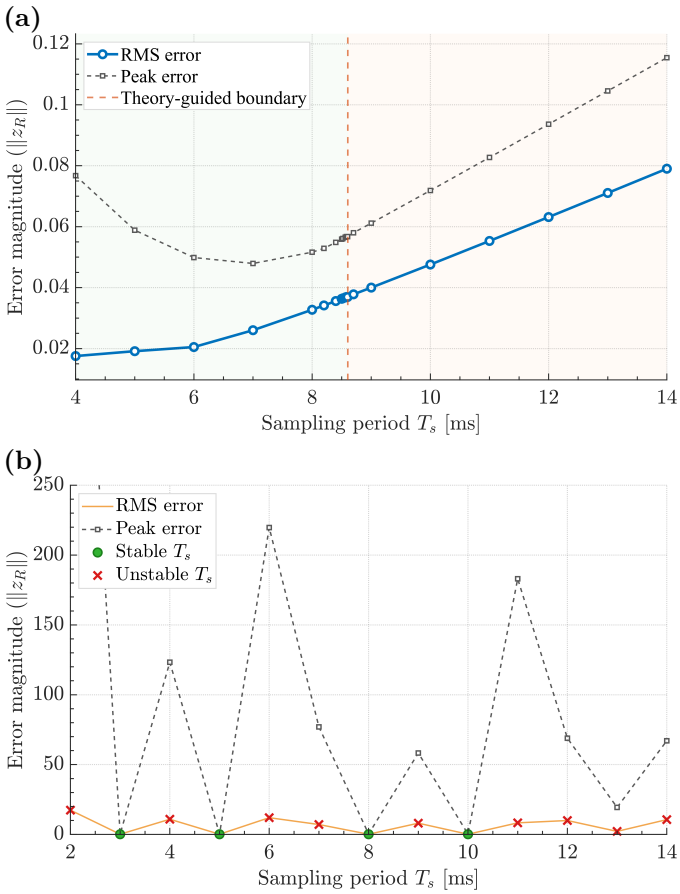


Fig. 9: Sampling-dependent tracking performance. **(a)** Direct DT: monotonic and predictable degradation within the admissible sampling region. **(b)** Emulation-based: non-monotonic and unpredictable behavior across sampling periods.

Future work will focus on extending the proposed framework to account for parametric uncertainties and external disturbances, as well as developing adaptive and robust extensions within the intrinsic DT geometric framework.

Appendix A
Translational Lyapunov Difference Derivations

This appendix provides detailed derivations of the discrete-time Lyapunov forward differences for the translational subsystem.

A. Derivation of the Position-Loop Lyapunov Difference

Starting from the closed-loop position error dynamics

$$\mathbf{e}_p(k+1) = (I - K_pT_s)\mathbf{e}_p(k) + T_s\mathbf{e}_v(k),$$

the position-loop Lyapunov function

$$V_P(k) = \frac{1}{2}\|\mathbf{e}_p(k)\|^2$$

yields the forward difference

$$\Delta V_P(k) = \frac{1}{2}\|\mathbf{e}_p(k+1)\|^2 - \frac{1}{2}\|\mathbf{e}_p(k)\|^2.$$

Substituting the closed-loop dynamics and expanding the quadratic terms gives

$$\begin{aligned}\Delta V_P(k) = &-\frac{1}{2}\mathbf{e}_p^\top(k)\big(2K_pT_s - K_p^2T_s^2\big)\mathbf{e}_p(k)\\ &+ T_s\mathbf{e}_p^\top(k)(I - K_pT_s)\mathbf{e}_v(k)\\ &+ \frac{1}{2}T_s^2\|\mathbf{e}_v(k)\|^2. \end{aligned} \tag{71}$$

B. Construction of $W_T(k)$

Using

$$V_T(k) = V_P(k) + \frac{1}{2}\|\mathbf{e}_v(k)\|^2,$$

the Lyapunov forward difference becomes

$$\Delta V_T(k) = W_T(k) + \frac{1}{2}\|\mathbf{e}_v(k+1)\|^2,$$

where

$$\begin{aligned}W_T(k) &= \Delta V_P(k) - \frac{1}{2}\|\mathbf{e}_v(k)\|^2\\ &= -\frac{1}{2}\mathbf{e}_p^\top(k)\big(2K_pT_s - K_p^2T_s^2\big)\mathbf{e}_p(k)\\ &\quad + T_s\mathbf{e}_p^\top(k)(I - K_pT_s)\mathbf{e}_v(k)\\ &\quad + \left(\frac{1}{2}T_s^2 - \frac{1}{2}\right)\|\mathbf{e}_v(k)\|^2. \end{aligned} \tag{72}$$

C. Coefficient Bounds after Young's Inequality

For any $\alpha > 0$, Young's inequality gives

$$\begin{aligned}T_s\mathbf{e}_p^\top(I - K_pT_s)\mathbf{e}_v \le &\frac{\alpha T_s}{2}\mathbf{e}_p^\top(I - K_pT_s)^\top(I - K_pT_s)\mathbf{e}_p\\ &+ \frac{T_s}{2\alpha}\|\mathbf{e}_v\|^2. \end{aligned} \tag{73}$$

Substituting this bound into $W_T(k)$ yields

$$W_T(k) \le c_1\|\mathbf{e}_p(k)\|^2 + c_2\|\mathbf{e}_v(k)\|^2,$$

where

$$\begin{aligned}c_1 = &-\frac{1}{2}\lambda_{\min}\Big(2K_pT_s - K_p^2T_s^2\Big)\\ &+ \frac{\alpha T_s}{2}\lambda_{\max}\Big((I - K_pT_s)^\top(I - K_pT_s)\Big),\\ c_2 = &\frac{1}{2}(T_s^2 - 1) + \frac{T_s}{2\alpha}. \end{aligned} \tag{74}$$

Appendix B
Derivation of the Residual Term in the $SO(3)$ Lyapunov Difference

This appendix clarifies the origin and bound of the residual term $r_R(k)$ appearing in the discrete-time Lyapunov difference of the rotational subsystem. The residual arises from the first-order truncation employed in the Lyapunov difference analysis on $SO(3)$, rather than from the structure-preserving discrete-time rotational model itself.

A. Exact Error Propagation on $SO(3)$

Using the exact structure-preserving discrete-time attitude kinematics of $\mathbf{R}(k)$ and $\mathbf{R}_d(k)$, the attitude error $\mathbf{R}_e(k) = \mathbf{R}_d^\top(k)\mathbf{R}(k)$ evolves as

$$\mathbf{R}_e(k+1) = \exp(-T_s\boldsymbol{\Omega}_d(k)^\wedge)\,\mathbf{R}_e(k)\exp(T_s\boldsymbol{\Omega}(k)^\wedge)\,, \tag{75}$$

which evolves intrinsically on the Lie group $SO(3)$ and introduces no modeling residual.

B. Lyapunov Difference and First-Order Expansion

Consider the geometric attitude error function

$$\Psi(\mathbf{R}_e) = \tfrac{1}{2}\operatorname{tr}(\mathbf{I} - \mathbf{R}_e). \tag{76}$$

The discrete-time Lyapunov difference is

$$\Delta V_R(k) = \Psi(\mathbf{R}_e(k+1)) - \Psi(\mathbf{R}_e(k)) = \tfrac{1}{2}\operatorname{tr}\big(\mathbf{R}_e(k) - \mathbf{R}_e(k+1)\big). \tag{77}$$

For sufficiently small sampling period T_s, the matrix exponential admits the first-order expansion

$$\exp(\pm T_sX^\wedge) = \mathbf{I} \pm T_sX^\wedge + O(T_s^2). \tag{78}$$

Applying this expansion to (75) yields

$$\mathbf{R}_e(k+1) = \mathbf{R}_e(k) + T_s(-\boldsymbol{\Omega}_d(k)^\wedge\mathbf{R}_e(k) + \mathbf{R}_e(k)\boldsymbol{\Omega}(k)^\wedge) + O(T_s^2). \tag{79}$$

Substituting into the Lyapunov difference and using the cyclic property of the trace operator gives

$$\Delta V_R(k) = T_s\,\mathbf{e}_R^\top(k)\big(\boldsymbol{\Omega}(k) - \mathbf{R}_e^\top(k)\boldsymbol{\Omega}_d(k)\big) + r_R(k), \tag{80}$$

where $r_R(k)$ collects all second-order and higher-order terms resulting from the truncation.

C. Residual Bound

Since the geometric error function $\Psi(\mathbf{R}_e)$ is smooth in a compact neighborhood of the identity, there exists a constant $c_R > 0$ such that

$$|r_R(k)| \le c_RT_s^2\big(\|\mathbf{e}_R(k)\|^2 + \|\mathbf{e}_\Omega(k)\|^2\big), \tag{81}$$

where

$$\mathbf{e}_\Omega(k) = \boldsymbol{\Omega}(k) - \mathbf{R}_e^\top(k)\boldsymbol{\Omega}_d(k).$$

Consequently, $|r_R(k)| \le \delta_R$ with $\delta_R = O(T_s^2)$, which justifies the residual bound adopted in Theorem 2.

Appendix C
Emulation-Based CT Baseline

This appendix summarizes the CT geometric backstepping controller used as a baseline in Section VI-D.

A. Control Law

1) Translational Subsystem: Define the tracking errors

$$\mathbf{e}_p = \mathbf{p} - \mathbf{p}_d, \tag{82}$$

$$\mathbf{v}_d = \dot{\mathbf{p}}_d - \mathbf{K}_p\mathbf{e}_p, \tag{83}$$

$$\mathbf{e}_v = \mathbf{v} - \mathbf{v}_d. \tag{84}$$

The desired thrust vector is defined as

$$\mathbf{F}_d = m\Big(-\ddot{\mathbf{p}}_d + g\mathbf{e}_3 + \mathbf{e}_p + \mathbf{K}_p(\mathbf{e}_v - \mathbf{K}_p\mathbf{e}_p) + \mathbf{K}_v\mathbf{e}_v\Big). \tag{85}$$

2) Rotational Subsystem: Define the attitude error as

$$\mathbf{R}_e = \mathbf{R}_d^\top \mathbf{R}, \tag{86}$$

$$\mathbf{e}_R = \frac{1}{2}(\mathbf{R}_e - \mathbf{R}_e^\top)^\vee. \tag{87}$$

The virtual angular velocity and angular velocity error are defined as

$$\boldsymbol{\Omega}_v = \mathbf{R}_e^\top \boldsymbol{\Omega}_d - \mathbf{K}_R \mathbf{e}_R, \tag{88}$$

$$\mathbf{e}_\omega = \boldsymbol{\Omega} - \boldsymbol{\Omega}_v, \tag{89}$$

with

$$\dot{\boldsymbol{\Omega}}_v = -\boldsymbol{\Omega}^\wedge \mathbf{R}_e^\top \boldsymbol{\Omega}_d + \mathbf{R}_e^\top \dot{\boldsymbol{\Omega}}_d - \mathbf{K}_R \dot{\mathbf{e}}_R. \tag{90}$$

The control torque is given by

$$\boldsymbol{\tau} = \boldsymbol{\Omega} \times (\mathbf{J}\boldsymbol{\Omega}) + \mathbf{J}\dot{\boldsymbol{\Omega}}_v - \mathbf{e}_R - \mathbf{K}_\omega \mathbf{e}_\omega. \tag{91}$$

References

[1] I. Colomina and P. Molina, "Unmanned aerial systems for photogrammetry and remote sensing: A review," *ISPRS Journal of Photogrammetry and Remote Sensing*, vol. 92, pp. 79–97, 2014.

[2] D. Floreano and R. J. Wood, "Science, technology and the future of small autonomous drones," *Nature*, vol. 521, no. 7553, pp. 460–466, 2015.

[3] M. Idrissi, M. Salami, and F. Annaz, "A review of quadrotor unmanned aerial vehicles: Applications, architectural design and control algorithms," *Journal of Intelligent & Robotic Systems*, vol. 104, no. 1, pp. 1–26, 2022.

[4] W. Gu, S. Primatesta, and A. Rizzo, "Robust adaptive control for aggressive quadrotor maneuvers via SO(3) and backstepping techniques," *Robotics and Autonomous Systems*, vol. 188, p. 104942, 2025.

[5] T. Lee, M. Leok, and N. H. McClamroch, "Geometric tracking control of a quadrotor UAV on SE(3)," in *49th IEEE Conference on Decision and Control (CDC)*, 2010, pp. 5420–5425.

[6] K. J. Astrom and B. Wittenmark, *Computer-Controlled Systems: Theory and Design*. Mineola, NY, USA: Dover Publications, 2011, reprint of the 3rd edition.

[7] D. Nesic and A. R. Teel, "A framework for stabilization of nonlinear sampled-data systems based on their approximate discrete-time models," *IEEE Transactions on Automatic Control*, vol. 49, no. 7, pp. 1103–1122, 2004.

[8] S. P. Bhat and D. S. Bernstein, "A topological obstruction to continuous global stabilization of rotational motion and the unwinding phenomenon," *Systems & Control Letters*, vol. 39, no. 1, pp. 63–70, 2000.

[9] Y. Zhao, L. Zhao, J. Yu, and Q.-G. Wang, "Discrete-time adaptive fuzzy command filtered backstepping control for quadrotor UAV systems: Theory and experiments," *IEEE Transactions on Fuzzy Systems*, vol. 32, no. 6, pp. 3618–3628, 2024.

[10] L. Wang, J. Chen, Y. Huang, Y. Zhu, and H. Pei, "Geometric attitude tracking control of quadrotor UAVs with adaptive extended state observers," *ISA Transactions*, vol. 160, pp. 289–297, 2025.

[11] D. Nešić and L. Grüne, "Lyapunov-based continuous-time nonlinear controller redesign for sampled-data implementation," *Automatica*, vol. 41, no. 7, pp. 1143–1156, 2005.

[12] D. Nesic and D. S. Laila, "A note on input-to-state stabilization for nonlinear sampled-data systems," *IEEE Transactions on Automatic Control*, vol. 47, no. 7, pp. 1153–1158, 2002.

[13] Y. Zhang, C. Wen, and Y. C. Soh, "Discrete-time robust backstepping adaptive control for nonlinear time-varying systems," *IEEE Transactions on Automatic Control*, vol. 45, no. 9, pp. 1749–1755, 2000.

[14] H. K. Khalil, *Nonlinear Systems*, 3rd ed. Upper Saddle River, NJ, USA: Prentice Hall, 2002.

[15] S. S. Ge, G.-Y. Li, and T. H. Lee, "Adaptive NN control for a class of strict-feedback discrete-time nonlinear systems via backstepping," in *Proceedings of the 40th IEEE Conference on Decision and Control*, vol. 4, 2001, pp. 3146–3151.

[16] M. B. Kobilarov and J. E. Marsden, "Discrete geometric optimal control on Lie Groups," *IEEE Transactions on Robotics*, vol. 27, no. 4, pp. 641–655, 2011.

[17] T. Lee, N. H. McClamroch, and M. Leok, "A lie group variational integrator for the attitude dynamics of a rigid body with applications to the 3D pendulum," in *Proceedings of the 2005 IEEE Conference on Control Applications*, 2005, pp. 962–967.

[18] X. Zheng and X. Yang, "Command filter and universal approximator based backstepping control design for strict-feedback nonlinear systems with uncertainty," *IEEE Transactions on Automatic Control*, vol. 65, no. 3, pp. 1310–1317, 2020.

[19] B. Xu, F. Sun, C. Yang, D. Gao, and J. Ren, "Adaptive discrete-time controller design with neural network for hypersonic flight vehicle via backstepping," *International Journal of Control*, vol. 84, no. 9, pp. 1543–1552, 2011.

[20] A. R. Teel and D. Nesic, "Input-to-state stability of networked control systems," *Automatica*, vol. 40, no. 12, pp. 2121–2128, 2004.

[21] E.-H. Zheng, J.-J. Xiong, and J.-L. Luo, "Second-order sliding mode control for a quadrotor UAV," *ISA Transactions*, vol. 53, no. 4, pp. 1350–1356, 2014.

[22] H. Voos, "Nonlinear control of a quadrotor micro-UAV using feedback linearization," in *2009 IEEE International Conference on Mechatronics*, 2009, pp. 1–6.

[23] B. Whitehead and S. Bieniawski, "Model reference adaptive control of a quadrotor UAV," in *AIAA Guidance, Navigation, and Control Conference*, 2010.

[24] H. Lee, S. Kim, T. Ryan, and H. J. Kim, "Backstepping control on SE(3) of a micro quadrotor for stable trajectory tracking," in *2013 IEEE International Conference on Systems, Man, and Cybernetics*, 2013, pp. 4522–4527.

[25] C. Liu, S. Yang, D. Luo, and J. Zhou, "Robust back-stepping controller on SO(3) for quadrotor attitude tracking," in *2018 10th International Conference on Modelling, Identification and Control (ICMIC)*, 2018, pp. 1–6.

[26] M. Wang, Z. Wang, Y. Chen, and W. Sheng, "Adaptive neural event-triggered control for discrete-time strict-feedback nonlinear systems," *IEEE Transactions on Cybernetics*, vol. 50, no. 7, pp. 2946–2958, 2020.

[27] Y.-J. Liu, L. Tang, S. Tong, and C. L. P. Chen, "Adaptive NN controller design for a class of nonlinear MIMO discrete-time systems," *IEEE Transactions on Neural Networks and Learning Systems*, vol. 26, no. 5, pp. 1007–1018, 2015.

[28] I. I. Hussein, M. Leok, A. K. Sanyal, and A. M. Bloch, "A discrete variational integrator for optimal control problems on SO(3)," in *Proceedings of the 45th IEEE Conference on Decision and Control*, 2006, pp. 6636–6641.

Data Availability

Data sharing is not applicable to this article as no datasets were generated or analyzed during the current study.

Author Contributions

Y.C. developed the methodology, carried out the theoretical analysis and simulations, and wrote the manuscript. A.R. supervised the research and revised the manuscript. All authors reviewed and approved the final manuscript.

Declarations

Competing Interests Alessandro Rizzo is a Senior Editor at Large of the Journal of Intelligent and Robotic Systems. The authors declare no additional conflicts of interest.

Yuan Cao is currently pursuing the Ph.D. degree in Electronics and Telecommunications at Politecnico di Torino, Turin, Italy. He received the B.Sc. degree in Mechanical Engineering in 2020 and the M.Sc. degree in

Mechatronic Engineering in 2022 from the same institution. His research focuses on adaptive and learning-based control, nonlinear and geometric control theory, and sensor fusion for UAVs and autonomous robotic systems, with particular interests in discrete-time control design and real-world robotic applications.

Alessandro Rizzo is an Associate Professor at the Department of Electronics and Telecommunications, Politecnico di Torino, Italy, where he coordinates the Complex Systems Laboratory. He received his Laurea degree in Computer Engineering, summa cum laude, and his PhD in Automation and Electronics Engineering from the University of Catania, Italy, in 1996 and 2000, respectively. Dr. Rizzo's previous affiliations include JET Joint Undertaking (UK), ST Microelectronics (Italy), the University of Messina (Italy), Politecnico di Bari (Italy), and New York University (USA). His research interests span complex networks and systems, robotics, and modeling and control of nonlinear systems. He has authored two books, holds two international patents, and has published over 200 papers in peer-reviewed international journals and conference proceedings. A Distinguished Lecturer for the IEEE Nuclear and Plasma Sciences Society, he received the Best Application Paper Award at the 2002 IFAC World Congress, as well as two Amazon Research Awards in Robotics (2019 and 2021).